In-situ measurements of molecular markers facilitate understanding of dynamic sources of atmospheric organic aerosols

Xiaopu Lyu[1], Hai Guo[1*], Dawen Yao[1], Haoxian Lu[1], Yunxi Huo[1], Wen Xu[2], Nathan Kreisberg[3], Allen H. Goldstein[4,5], John Jayne[2], Douglas Worsnop[2], Yan Tan[1], Shun-Cheng Lee[1], Tao Wang[1]

[1] Department of Civil and Environmental Engineering, Hong Kong Polytechnic University, Hong Kong

[2] Center for Aerosol and Cloud Chemistry, Aerodyne Research Inc., Billerica, MA 01821

[3] Aerosol Dynamics Inc., Berkeley, CA 94710

[4] Department of Environmental Science, Policy, and Management, University of California, Berkeley, CA 94720

[5] Department of Civil and Environmental Engineering, University of California, Berkeley, CA 94720

*Corresponding author. ceguohai@polyu.edu.hk

Abstract: Reducing the amount of organic aerosol (OA) is crucial to mitigation of particulate pollution in China. We present time and air-origin dependent variations of OA markers and source contributions at a regionally urban background site in South China. The continental air contained primary OA markers indicative of source categories, such as levoglucosan, fatty acids and oleic acid. Secondary OA (SOA) markers derived from isoprene and monoterpenes also exhibited higher concentrations in continental air, due to more emissions of their precursors from terrestrial ecosystems and facilitation of anthropogenic sulfate for monoterpenes SOA. The marine air and continental–marine mixed air had more abundant hydroxyl dicarboxylic acids (OHDCA), with anthropogenic unsaturated organics as potential precursors. However, OHDCA formation in continental air was likely attributable to both biogenic and anthropogenic precursors. The production efficiency of OHDCA was highest in marine air, related to the presence of sulfur dioxide and/or organic precursors in ship emissions. Regional biomass burning (BB) was identified as the largest contributor of OA in continental air, with contributions fluctuating from 8% to 74%. In contrast, anthropogenic SOA accounted for the highest fraction of OA in marine (37±4%) and mixed air (31±3%), overriding the contributions from BB. This study demonstrates the utility of

molecular markers for discerning OA pollution sources in the offshore marine atmosphere, where continental and marine air pollutants interact and atmospheric oxidative capacity may be enhanced.

Keywords: Secondary organic aerosols; Biomass burning; Source apportionment; Ship emission; Hydroxyl dicarboxylic acids

1. Introduction

Organic aerosol (OA) constitutes a considerable fraction (20-90% globally) of airborne fine particulate matters (PM) [1, 2], and is considered to significantly account for haze occurrence [3, 4], climatic consequences [1, 5] and impairments to health [6]. Despite successful efforts to decrease nationwide fine PM loadings in China, reducing OA has been a major obstacle for China to win the battle against air pollution [3, 7]. This is mainly due to insufficient understanding of OA, particularly the rapidly changing and spatially diverse contributions of primary (POA) and secondary (SOA) sources [8, 9].

To identify sources of OA and quantify their contributions, receptor models based on known tracers of specific sources are widely adopted [3, 10]. The filter-based technique makes use of fine PM collected and accumulated on filters, which are chemically characterized following solvent extraction (SE) [11, 12] or thermal desorption (TD) [13]. Data obtained from filters are generally of low time resolution (12 – 24 hours) [11-13]. While filter-TD can substantially enhance ease of laboratory analysis, it performs poorly in analysis of polar organic compounds, unless online derivatization is utilized [13, 14]. As an alternative, Aerosol Mass Spectrometry (AMS) is extensively used in source apportionment of OA, based on the fast detection of OA at resolution of minutes [15, 16]. However, the AMS-based technique usually fails to identify specific sources of OAs [15, 16], due to the lack of compound based separation during analysis and the chemical similarity of many source markers with each other. Overall, there is a present challenge to determine the continuously changing (rather than average) contributions of specific (rather than lumped) sources to ambient OA.

Hong Kong in South China is an Asian metropolis, with tertiary industries (*e.g.* financial service and tourism) as the main economic pillars. Restaurants are scattered throughout every corner of the city, supplying a mix of Chinese and western foods. The city is also known for its heavy traffic,

i.e. more than 300 licensed vehicles per km of road. With a population of 7.4 million and a land area of merely 1.1×10^3 km^2, the air in Hong Kong is polluted by many local sources. Additionally weather driven forces affect Hong Kong air quality with southern winds from the South China Sea (SCS) providing cleaner air to Hong Kong in the summer, while the continent-originated northern winds deteriorate air quality in winter [17-19]. The meso-scale circulations and emissions in microenvironments also modulate air quality [18-20]. These factors may explain the discrepancies in the sources of OA or source contributions reported in previous studies [21-24]. For example, cooking emissions have been determined to explain more than 30% (~3.6 μg m^{-3}) of OA at a roadside site in Hong Kong using AMS and Aerosol Chemical Speciation Monitoring data [21-22], which however were not resolved or identified with much lower contributions (1.2%, ~0.2 μg m^{-3}) in many other places by filter-based source apportionment [23-24]. Hu et al. [23] argued that biomass burning (BB) contributed ~38% (3.6 μg m^{-3}) to OA at 4 suburban sites in Hong Kong with the intrusion of regional air, including 2.2 μg m^{-3} of BB-related POA and 1.4 μg m^{-3} of BB-induced SOA. In cool seasons when Hong Kong received regional air from mainland China, the BB contributions (1.6 μg m^{-3}) were even comparable to those of vehicle emissions (1.5 μg m^{-3}) at a suburban site [24]. Nevertheless, this finding was not supported by AMS-based source apportionment which did not identify BB as a significant source of OA in either suburban or roadside environments [15, 21-22]. Besides, the sum of SOA components resolved by filter-based approach was not always comparable in concentration to the total oxygenated organic aerosol (OOA) determined by AMS [15, 21-24]. In addition to the changing atmospheric conditions and emissions, methodological differences might be another reason for the discrepancies. Hence, to better understand the driving forces of poor air quality in Hong Kong, it is necessary to determine specific sources of OA with higher time- and space-resolution, by combining the advantages of filter-based and AMS-based source apportionment techniques.

Thermal-desorption Aerosol Gas-chromatograph (TAG), an in-situ chemical marker oriented instrument, has been developed for time resolved analysis of organic molecular makers and is increasingly applied in OA studies [25-28]. Table S1 lists the development and representative application of different versions of TAG, including impactor TAG, 2D-TAG, SV-TAG and TAG-AMS developed by US groups [29-35], and Q-TAG, Dual-trap TAG and 2D-Q-TAG developed by a China group [36-38]. The main findings of the application are summarized in Table S1, and we also briefly commented on the performance of the instruments. Overall, TAG families have

contributed to comprehensive measurements of semi-volatile, intermediate-volatility and condensed organic compounds [27], study on gas/particle partitioning [25], identification of sources of airborne organics [28], and research on SOA formation mechanisms [26]. In this study, a modified impactor TAG with in-situ calibration, on-line derivatization and high-resolution time-of-flight mass spectrometry analysis, which provided in-situ measurement of both polar and non-polar OA markers every 1.5 hours, was applied to analyze the molecular composition of OA in Hong Kong. The specific sources of OA and their dynamics were determined in air masses of different origins. Intense formation of anthropogenic SOA in relatively clean air was also demonstrated. This paper presents a reliable method of tracking the sources of POA and formation processes of SOA in abrupt and transient pollution events, which should assist policy-makers in taking actions against spikes in fine PM pollution.

2. Overview of sampling campaign

In November–December 2018, a sampling campaign was carried out at a relatively remote coastal site at the southeast tip of Hong Kong (Figure S1) to study the photochemical air pollution in this highly urbanized subtropical region. Though it is located in Hong Kong, the site has long been regarded as a regionally urban background site in South China, given that air pollutants in the adjoining Pearl River Delta reached the site within a few hours [39, 40]. A **T**hermal desorption **A**erosol **G**as chromatograph – **T**ime **o**f **F**light – **M**ass **S**pectrometer (TAG-Tof-MS, hereinafter referred to as TAG) was deployed to measure the OA markers in airborne PM_1 (PM with aerodynamic diameters less than 1 μm) during 13 November–19 December. PM_1 was focused to match the data analyzed by Aerosol Mass Spectrometer, which is introduced below. Figure 1 shows a schematic of TAG. Fine PM was sampled through a PM_1 cyclone to eliminate coarse particles above 1 μm before collection in an inertial impactor based collection and thermal desorption (CTD) cell. Collected samples were thermally desorbed from 30 to 315 °C into helium. To improve analysis of polar compounds, silylation derivatization was performed in-situ simultaneously with desorption using helium purge flow ~80% saturated with a sylating reagent (N-Methyl-N-(trimethylsilyl)trifluoroacetamide, MSTFA) (DVZ). All the desorbed species were directed through a secondary focusing trap (FT), where the target compounds were trapped and the high volatility species including excess MSTFA were vented. Next, the FT was heated and back-flushed with helium to transfer trapped species to the miniature gas chromatograph for

chemical analysis. A low-polarity metal column with length of 20 m (Restek, Cat. # 71822) was used for analysis with the column flow controlled by an electronic pressure controller (EPC). In this campaign, the TAG was operated at the resolution of 1.5 hours per sample. The continuous measurement was interrupted by instrument maintenance in some time slots. Polar compounds were not detected between 22 November 12:00 and 26 November 19:00, due to running out of MSTFA. The operation procedures of TAG are elaborated in Text S1 and Table S2.

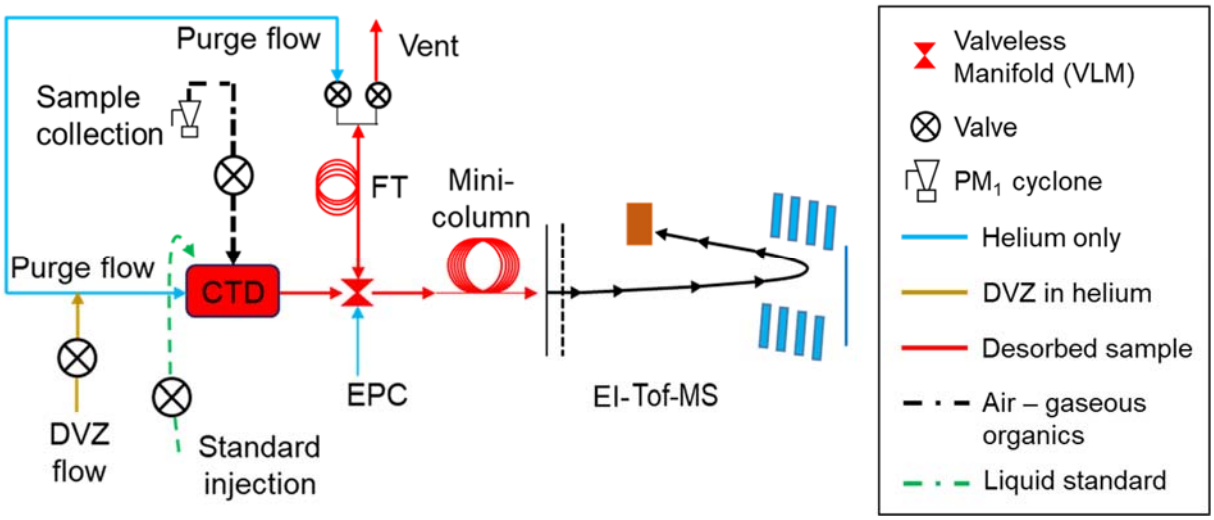

Figure 1. Schematic of TAG. The term "Air – gaseous organics" means air samples with the gaseous organics being removed by a carbon denuder (not shown) and coarse particles removed by PM_1 cyclone. DVZ: derivatization; CTD: collection and thermal desorption cell; FT: focusing trap; EPC: electronic pressure controller; EI-Tof-MS: electron impact–time of flight–mass spectrometer.

Throughout the field campaign, 66 compounds with the volatilities spanning C_{13}–C_{35} *n*-alkanes in 478 valid samples were quantified by TAG, with the use of internal and authentic/surrogate standards. A mix of 41 deuterated compounds was adopted as internal standards in analysis of each sample and in calibration, to track and correct the changes in instrumental sensitivity. In this study, we focused on 40 out of 66 quantified organic compounds, which were routinely at detectable concentrations and indicative of OA sources. The detection rates were lower than 75% for the other 26 compounds. Table S3 lists the average concentrations of the 40 organic compounds, with the quantification ions, internal standards, surrogate standards, and quality control metrics. To facilitate discussion, the 40 OA compounds were grouped according to their chemical structures,

potential sources and correlations. Table S4 shows the 15 species groups, including isoprene SOA tracers (Isop-SOA-T), monoterpene SOA tracers (MT-SOA-T), saccharides, hydroxyl dicarboxylic acids (OHDCA), hydroxyl benzoic acids (OHBA), even *n*-alkanes type 1 & 2 (even *n*-alk1&2), odd *n*-alkanes type 1 & 2 (odd *n*-alk1&2), even fatty acids (even FA), 2,3-dihydroxy-4-oxopentanoic acid (DHOPA), vanillic acid (VA), mannosan, levoglucosan and oleic acid. Both the even and odd *n*-alkanes were divided into two types, due to the potentially different sources. The species in each group were at least moderately correlated, with R^2 higher than 0.7. A majority of the 15 groups were used as tracers in OA source apportionment, and the rationalities and uncertainties are elaborated in section 3.3.

Additionally, a **H**igh **R**esolution – **T**ime **o**f **F**light – **A**erosol **M**ass **S**pectrometer (Aerodyne Research Inc. HR-Tof-AMS, hereinafter referred to as AMS) was applied to analyze the non-refractory composition of PM_1, including sulfate, nitrate, ammonium, chloride and total organic matter (OM). Text S2 illustrates the calibration and measurement configurations of the AMS. The collection efficiency of 0.73 (Text S2 and Figure S2) was applied to the concentrations of all PM_1 components. In this study, five-minute averaged W-mode data was used. It is worth noting that AMS data were not available after 7 December, due to malfunction of the chopper. Moreover, additional air pollutants and meteorological conditions were monitored by the Hong Kong Environmental Protection Department (HKEPD) and other research groups. Table S5 summarizes the instruments for these auxiliary measurements.

3. Results and Discussion

3.1 Time and air-origin dependent concentrations of OA markers

Throughout the field campaign, the origins of air masses arriving at the sampling site (Hok Tsui, HT) were examined. Analysis of the daily clustered 72 hour backward trajectories (not shown) indicated that the air parcels originated from either the continent or SCS, labeled as continental and marine air, respectively. For the former, some trajectories passed over SCS before reaching HT, representing a mix of continental and marine air. Figure 2 shows the distribution of air mass concentrations for the three types of air. Continental air accounted for the largest fraction (~60%) of the sampled air, with the rest being equally constituted by marine (~20%) and mixed air (~20%). The east part of Guangdong (GD), central and southern Jiangxi (JX) and coastal area of Fujian (FJ) were the main points of origin of the continental air. While the mixed air was still partially

stemming from GD and JX, the back trajectories showed mainly offshore origins for marine air. The uncertainties in further analyses related to the classification of air mass origins are discussed in Text S3.

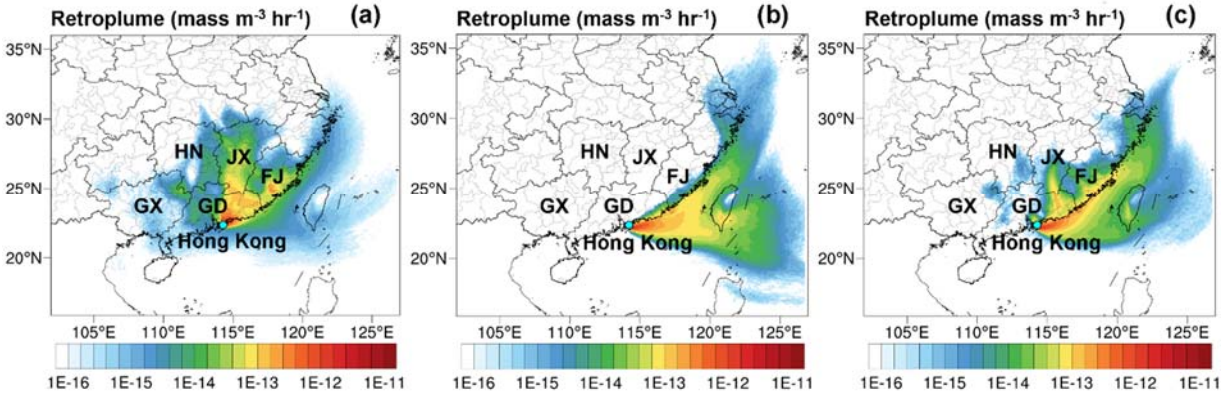

Figure 2. Distribution of air mass concentrations (in unit of mass m^{-3} hr^{-1}) in (a) continental, (b) marine and (c) mixed air masses within 500 m during 13 November–19 December 2018, according to the HYSPLIT Lagrangian backward particle release simulation at HT (22.209 N, 114.253 E). GD: Guangdong; GX: Guangxi; FJ: Fujian; HN: Hunan; JX: Jiangxi. Hong Kong is symbolized by the blue circle.

Among the quantified OA markers, OHDCA group exhibited the highest concentrations (266±17 ng m^{-3}), dozens to hundreds of times higher than those of the other OA markers. Malic acid and two isomers of tartaric acid were the main components of OHDCA. The concentration of malic acid (most abundant individual specie) ranged from 9 ng m^{-3} to 517 ng m^{-3}, with a mean of 119±8 ng m^{-3}. These were at the same magnitude as those observed [41] at an urban site in Hong Kong in summer (mean: 192 ng m^{-3}; maximum: 662 ng m^{-3}) and those reported [42] at another urban site in winter (mean: 155 ng m^{-3}; maximum: 179 ng m^{-3}). The concentrations of two isomerized tartaric acids were 76±5 ng m^{-3} and 67±4 ng m^{-3}, respectively. Levoglucosan, as a BB tracer [43], ranked highest in concentration (12±1 ng m^{-3}) among the OA markers except OHDCA. However, the average concentration of levoglucosan was lower than 30 ng m^{-3} measured at the same site in autumn of 2001 [44] and 67 ng m^{-3} at a mountainous site in autumn of 2010 [17]. The increasingly stringent prohibition of field fires might account for the lower concentrations of levoglucosan observed in this campaign. As listed in Table S4, the SOA tracers were of relatively low concentrations, regardless of DHOPA derived from anthropogenic precursors [45] (0.4±0.02 ng m^{-}

193 ^{3}) or biogenic SOA tracers (Isop-SOA-T: 5.1±0.4 ng m^{-3}; MT-SOA-T: 1.7±0.1 ng m^{-3}). However,
194 this was not necessary to indicate low SOA fraction in PM_1-bounded OM (PM_1-OM, measured by
195 AMS in this study), due to the incomplete analysis of SOA compounds and the unknown origin of
196 OHDCA, as discussed later.

197 Figure 3 presents the time series of OA markers and PM_1-OM, along with black carbon (BC), PM_1
198 and meteorological parameters. It is notable that OHDCA concentrations were significantly higher
199 in the earlier phase of the sampling campaign (before 7 December), when the temperature was
200 relatively high (mean of 22±0.1 °C compared to 17±0.2 °C in the later phase). The Isop-SOA-T
201 and MT-SOA-T were also enhanced in the earlier phase. Conversely, most primary OA markers,
202 such as levoglucosan, *n*-alkanes, fatty acids and oleic acid (cooking emission tracer [46]), were
203 substantially built up in the later phase coincident with the dominance of continental air, indicating
204 a rise of POA fraction in PM_1-OM. In view of the concurrent spikes of BC, we infer that the POA
205 enhancements were likely attributable to transport, associated with the passing of a cold front on
206 7 December (Figure S3) which brought in continental air in the following days. The same
207 phenomena were observed after another cold front passed Hong Kong on 21 November (Figure
208 S3), with obvious enhancements of PM_1 and PM_1-OM. Carbon preference index (CPI) and the
209 mixing ratios of acetonitrile (gas phase BB indicator [47]) increased as well (Figure S4). Besides,
210 no correlation with either total or individual even FA implied that the m/z 60 and m/z 73 ions
211 detected by AMS were more related to BB in this campaign, in line with previous studies [48]. The
212 concentrations of both ions increased notably during 22–25 November (Figure S4). All these
213 signatures indicated the arrival of BB plumes with continental air induced by the shifting cold
214 front. This process might also apply to the other POA components. The cross-validation between
215 CPI (TAG data) and m/z 60, 73 (AMS data) during the plateau period, in combination with the
216 quality control metrics in Table S3, confirmed the robustness of OA markers measured by TAG.
217 Furthermore, the simultaneous increases of CPI and levoglucosan during 6–7 December (Figure
218 S4) implied the enhanced contributions of BB to PM_1-OM caused by the second cold front, though
219 the rise in CPI was less significant due to the concurrent enhancement of vehicle emissions (section
220 3.3).

221 Note that the correlation between levoglucosan and acetonitrile (particle and gas phase BB tracers,
222 respectively) was undermined by high levoglucosan concentrations observed with low

temperatures (<20.4 °C, median temperature), and levoglucosan inversely correlated (R = -0.79) with temperature (Figure S5). It was plausible that the shift of gas-to-particle partitioning also accounted for the elevated concentrations of some POA components (*e.g.* levoglucosan) in the continental air induced by cold fronts.

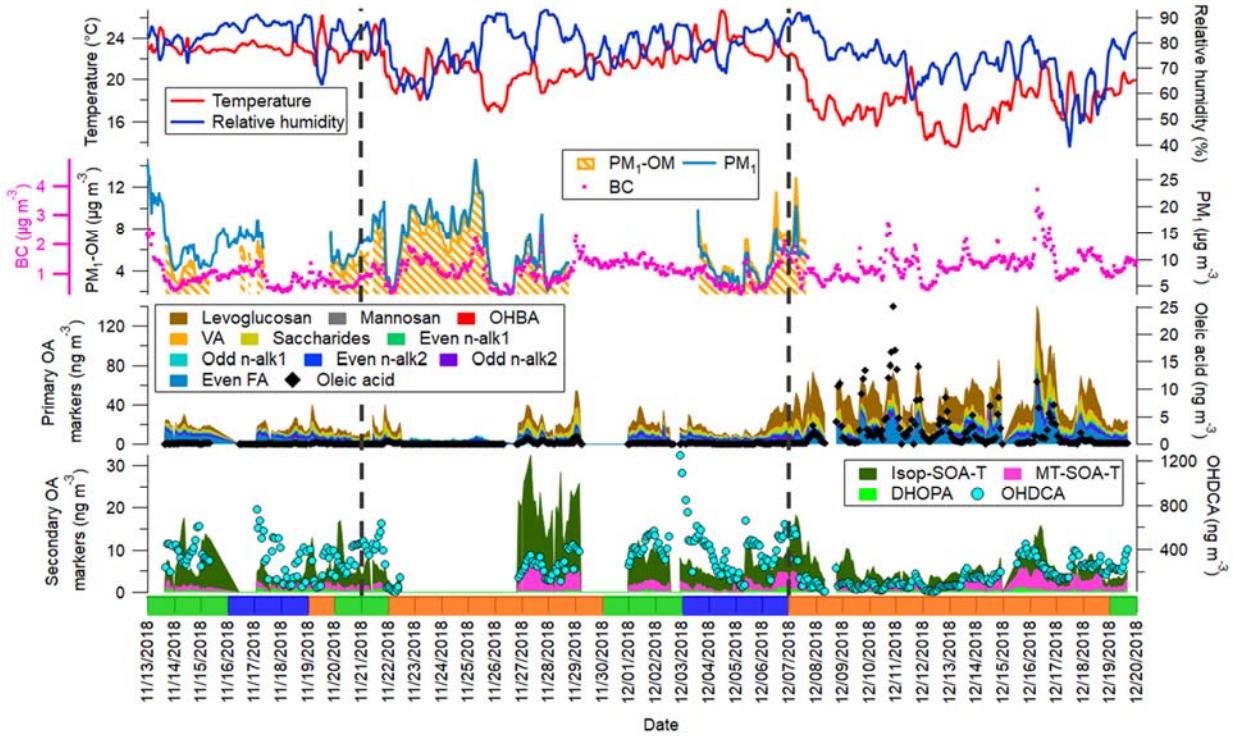

Figure 3. Time series of meteorological conditions, black carbon (BC), PM_1 and PM_1 compositions (including OA markers). Orange, green and blue bars on bottom axis denote continental, mixed and marine air, respectively. Black dashed lines indicate dates when cold fronts passed Hong Kong. Missing data are caused by maintenance of the instruments, except for the unavailable polar compounds during 22 November 12:00–26 November 19:00 due to running out of MSTFA.

Generally, the concentrations of OA markers were closely associated with air mass type, as listed in Table 1. An exception was isoprene, which exhibited comparable levels in all types of air masses. This was likely attributable to the dominance of local emissions in isoprene sources regardless of air mass origins, and/or inhibited isoprene emissions from terrestrial system in cool season. The local emissions might also partially account for the observed mixing ratios of monoterpenes and toluene in marine and mixed air, which were lower than those in continental air but were still of

significant levels. Under the assumption that local emissions were relatively consistent, the comparisons in Table 1 still reveal different air pollution features for different air mass types.

The continental air was laden with mostly primary air pollutants and POA tracers, such as carbon monoxide (CO), levoglucosan, fatty acids and oleic acid. Many other species not listed here, *e.g.* nitrogen oxides (NO_x), BC and *n*-alkanes, also exhibited higher concentrations in continental air. BB, vehicle exhaust and cooking emissions were the most likely sources. Despite the expected suppression of atmospheric oxidative capacity by NO_x [49, 50], the continental air still contained the largest amount of MT-SOA-T, attributable to higher background concentrations (section 3.2), more abundant monoterpenes as precursors (159±4 pptv) and enhanced formation of MT-SOA-T facilitated by sulfate (section 3.2). The marine air was characterized by the highest level of SO_2, indicating the impact of ship emissions. Isop-SOA-T was most deficient in marine air, despite little dependence of isoprene mixing ratios on air mass types, perhaps suggesting minor influence of local photo-oxidation of isoprene on Isop-SOA-T levels and/or higher background levels in continental and mixed air (section 3.2). Ozone (O_3) and OHDCA were somehow more abundant in marine air than in continental air, though they were even more prevalent in mixed air. This might be explained by the enhancement of oxidative capacity in offshore marine atmosphere (OMA), with the ageing of continental air in a NO_x-deficient atmosphere [51, 52]. Therefore, photo-degradation likely dominates production of OHDCA. The slightly lower levels of O_3 and OHDCA in marine air than in mixed air might be due to the lower abundance of reactants involved in photo-oxidation.

Table 1. Mean levels of OA markers (italic, ng m^{-3}) and trace gases including volatile organic compounds (VOCs) (ppbv unless otherwise specified) by air mass origins.

Species	Continental air	Marine air	Mixed air
O_3	39.2 ± 2.3	52.6 ± 2.0	65.3 ± 2.3
CO	372 ± 9	263 ± 11	260 ± 15
SO_2	1.1 ± 0.1	1.5 ± 0.1	1.3 ± 0.1
Isoprene	1.6 ± 0.04	1.5 ± 0.05	1.7 ± 0.1
Monoterpenes (pptv) *	159 ± 4	130 ± 4	142 ± 4
Toluene	3.3 ± 0.1	2.0 ± 0.1	1.9 ± 0.1
OHDCA	*183 ± 16*	*355 ± 38*	*384 ± 33*
Isop-SOA-T	*5.9 ± 0.7*	*3.8 ± 0.3*	*5.8 ± 0.7*
MT-SOA-T	*2.1 ± 0.2*	*1.1 ± 0.2*	*1.3 ± 0.1*

Levoglucosan	*16.9 ± 1.1*	*5.0 ± 1.0*	*5.4 ± 0.7*
Even fatty acids	*10.6 ± 1.0*	*4.6 ± 0.4*	*5.1 ± 0.6*
Oleic acid	*2.0 ± 0.5*	*0.2 ± 0.02*	*0.2 ± 0.02*

* Sum of monoterpenes detected by a Proton Transfer Reaction Quadrupole ion Time-of-Flight Mass Spectrometry. The molecular formula of the protonated compounds is $(C_{10}H_{16})H^+$, according to the parent ion of m/z 137.13248.

3.2 Diurnal patterns and correlation analysis

3.2.1 Diurnal patterns of OA markers

Diurnal pattern is a reflection of the evolution, sources and vertical mixing of air pollutants in a day. Figure 4 shows the diurnal variations of several typical OA markers. Both OHDCA and MT-SOA-T followed the diurnal pattern of O_x ($O_3 + NO_2$) (Figure S6), showing peaks in the afternoon, indicating their secondary origin. Although many OHDCA are extensively present in fruits and are used as food additives [53], they are also considered to be the late oxidation products of unsaturated hydrocarbons and fatty acids, and aldehydes [54, 55]. The O_x-like diurnal pattern suggested that OHDCA observed in this campaign were more likely to be derived from photo-oxidation.

Interestingly, Isop-SOA-T did not show analogous patterns to those of MT-SOA-T or O_x. The Isop-SOA-T concentrations were higher at night and lowest at noon, consistent with the diurnal development of Planetary Boundary Layer (PBL) (Figure S6). Isoprene, as the precursor of Isop-SOA-T, however had typical peaks at around 13:00 – 15:00 (not shown). Therefore, it was plausible that the detected Isop-SOA-T was a regional background signal more influenced by PBL height than by daytime photo-oxidation. This was verified by the smallest differences in Isop-SOA-T concentrations between marine air and continental/mixed air at noon, when the PBL was fully developed. In fact, there was a discernable increase for Isop-SOA-T in marine air during 01:00 – 07:00. This was also interpretable, given that the air above marine boundary layer might be of continental origin and the air rich in Isop-SOA-T intruded into the marine boundary layer where the background Isop-SOA-T was less abundant. However, the possibility that some dark reactions [56, 57] contributed to the higher nocturnal Isop-SOA-T cannot be ruled out.

The diurnal patterns of levoglucosan in continental air were opposite to the variations of temperature, likely resulting from the gas-to-particle partitioning. However, unusual increases

were observed for levoglucosan from 1:00 to 09:00 – 11:00 in marine and mixed air, which were analogous to the rise of Isop-SOA-T in marine air in the early morning. Therefore, the development of PBL and consequent air mixing caused the enhancement of levoglucosan in marine and mixed air before 09:00 – 11:00. Again, the smallest differences of levoglucosan concentrations among different air masses were also observed at noon, confirming the modulation of levoglucosan concentration by PBL development. A previous study [38] implied the downward transport of levoglucosan at the same site with the Philippines as potential source region in spring. While the vertical mixing still existed, the source regions might be different in our study, due to the very few air masses originating from or passing the Philippines (Figure 2).

Lastly, the diurnal patterns of oleic acid in continental air were also noteworthy, with an obvious peak during 19:00 – 21:00 (Figure S6). This coincides with the dining habits of Hong Kong people – big dinner and simpler breakfast and lunch.

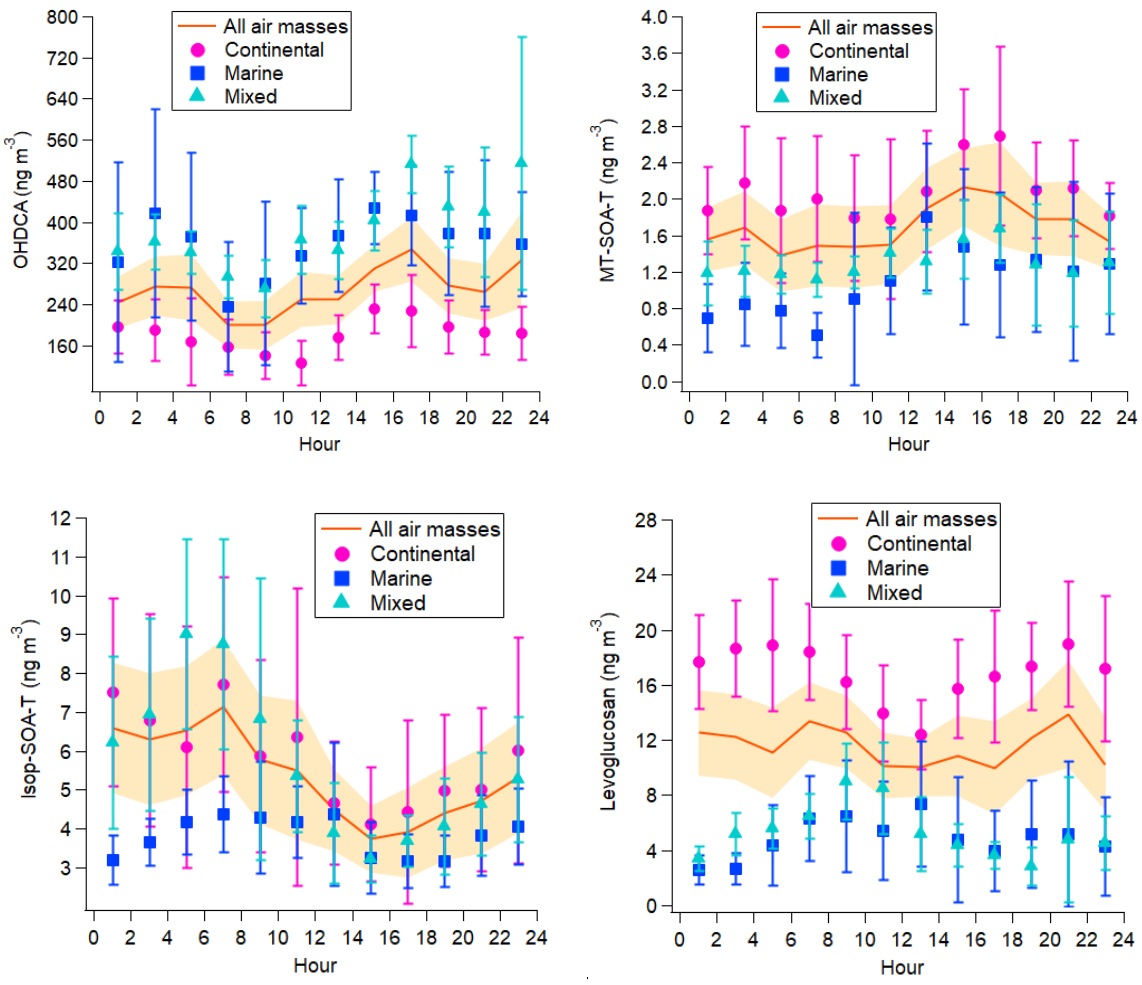

Figure 4. Average diurnal cycles of OHDCA, MT-SOA-T, Isop-SOA-T and levoglucosan in different air masses. Error bars and shaded area represent 95% confidence intervals (CIs).

3.2.2 Correlations of SOA markers with O_x

To further understand the formation processes of OHDCA and MT-SOA-T, correlation analyses were performed. Figure 5 shows the correlations of OHDCA *vs.* O_x and MT-SOA-T *vs.* O_x in different air masses. The moderate correlations between OHDCA and O_x reaffirmed the secondary source of OHDCA. Further correlation analysis found that OHDCA moderately (R^2=0.44) correlated with DHOPA (aromatics SOA) and fairly well (R^2=0.73) with MT-SOA-T in continental air. However, the correlations became much weaker in marine and mixed air. Nearly no correlation was identified between OHDCA and Isop-SOA-T in any type of air. Therefore, OHDCA in continental air might be derived from both anthropogenic and biogenic precursors, while it was likely attributable to anthropogenic precursors other than aromatics in marine and mixed air. The inferences were reasonable for individual compounds included in the group of OHDCA (Table S4), except for citramalic acid (CMA) and 2-hydroxyglutaric acid (2-HGA) which might be partially derived from biogenic VOCs in marine air due to their good correlations with MT-SOA-T (R^2=0.65 and 0.72, respectively). However, CMA and 2-HGA only constituted 0.5% and 1.4% of OHDCA in mass concentration, respectively. This supports the argument of Hu and Yu [42], who indicated that only in summer were biogenic VOCs the main precursors of OHDCA in Hong Kong.

Furthermore, the slope of OHDCA *vs.* O_x in marine air was highest among the three regressions, and we found that the high levels of OHDCA in marine air were generally accompanied by elevated SO_2 concentrations. The SO_2 spikes in marine air most likely related to ship emissions, which has become the largest source of SO_2 in Hong Kong [58]. It was therefore plausible that the production efficiency of OHDCA was enhanced in marine air with ship emissions. On one hand, ship emissions might consist of high levels of some OHDCA precursors not detected by us. On the other hand, it remains to be verified whether SO_2 in ship emissions facilitates the formation of anthropogenic SOA.

For MT-SOA-T, the correlation with O_x was weakest in continental air. It is interesting to note that the samples away from the regression line generally had high concentrations of sulfate in $PM_{2.5}$, implying the well-documented catalysis of acidic aerosols to formation of biogenic SOA [59].

Besides, the larger intercept in "continental" regression suggested higher background MT-SOA-T in continental air. The correlation of MT-SOA-T *vs.* O_x in marine air was somewhat undermined by several samples with high BC levels, possibly due to the intrusion of continental air. Regressions excluding these samples achieved better correlations with a slope closer to those acquired in "continental" and "mixed" regressions. As such, the formation of MT-SOA-T was not enhanced in marine air. This reduced the possibility that SO_2 in ship emissions accelerated the formation of SOA (*e.g.* OHDCA), but further studies are needed for confirmation. Nevertheless, the lower concentrations of MT-SOA-T in marine and mixed air were mostly attributable to the gaps in background levels, rather than different oxidation efficiencies.

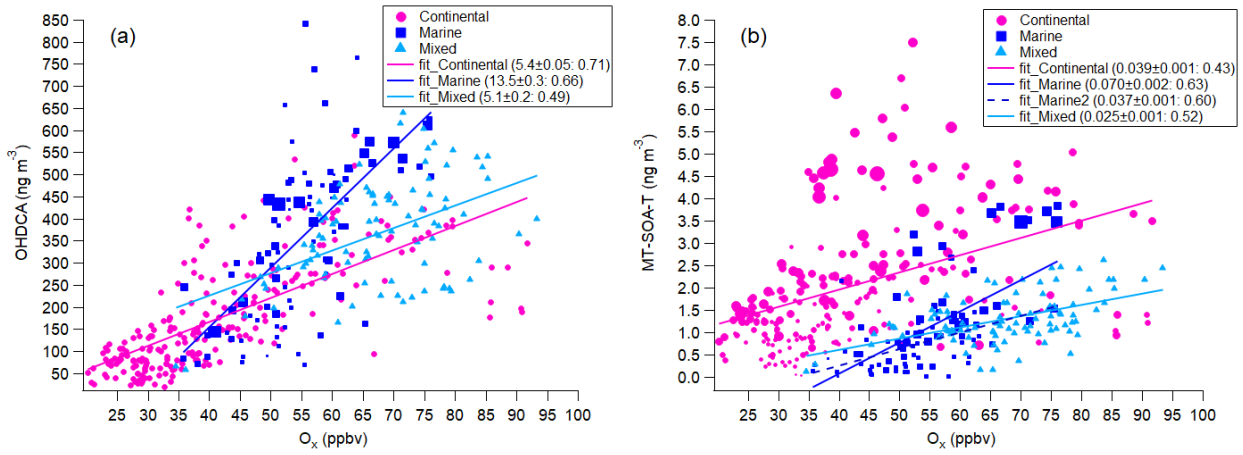

Figure 5. Correlations of (a) OHDCA *vs.* O_x, and (b) MT-SOA-T *vs.* O_x by air mass origins. Size of square markers in (a) is proportional to SO_2 concentration. Size of circles and squares in (b) is proportional to sulfate level in $PM_{2.5}$ and BC, respectively. Numbers in parentheses are (slope: correlation coefficient). Blue dashed line in (b) indicates the regression excluding data points with high BC concentrations.

3.3 Sources of PM_1-OM

With provision of time resolved concentrations of organic molecular markers, TAG data assisted to identify dynamic and specific sources of OA [28, 60-63] and other PM bound components (*e.g.* BC) [64]. Figure 6 shows the source profiles of PM_1-OM resolved by US Environmental Protection Agency's Positive Matrix Factorization model (v 5.0.12). A PMF solution of 6 factors was adopted, according to the metrics of Q/Q_{exp} (Figure S7) and the interpretability of source profiles (Figures

6 & S8), as illustrated in Text S4 where the model configurations, residual analysis (Figure S9) and error estimates are also presented.

The first factor was defined as secondary sulfate, due to the dominance of sulfate and ammonium. 8% of PM_1-OM and moderate fractions of saccharides and *n*-alkanes were also allocated in this factor, partially constituting the unresolved OMs due to the lack of OA markers for some sources (such as hopanes indicative of vehicle emissions [65]). The second and third factors had exclusively high loading of Isop-SOA-T and MT-SOA-T, representing isoprene SOA and monoterpenes SOA, respectively. The fourth factor was characterized by OHDCA and DHOPA, both of which are SOA components. As discussed above, anthropogenic VOCs were most likely precursors of OHDCA in marine and mixed air. Though OHDCA in continental air might also be derived from biogenic VOCs, the concentrations were only half of those in marine and mixed air (Table 1). CMA and 2-HGA partially of biogenic origins in marine air had very low mass fractions (<2%) in OHDCA. Besides, DHOPA is generally considered to be an oxidation product of aromatics [66]. Hence, this factor was tentatively identified as anthropogenic SOA. The fifth factor was dominated by BB tracers, such as levoglucosan, mannosan and vanillic acid [67], thereby representing biomass burning OA (BBOA). Moderate loadings of nitrate, ammonium and chloride presented in the last factor, which was termed as secondary nitrate. 24% of PM_1-OM was attributed to this factor, being another part of unresolved OMs. The concentrations of oleic acid were below detection limit in 51% samples, and were not included in source apportionment. Hence, cooking OA was not identifiable.

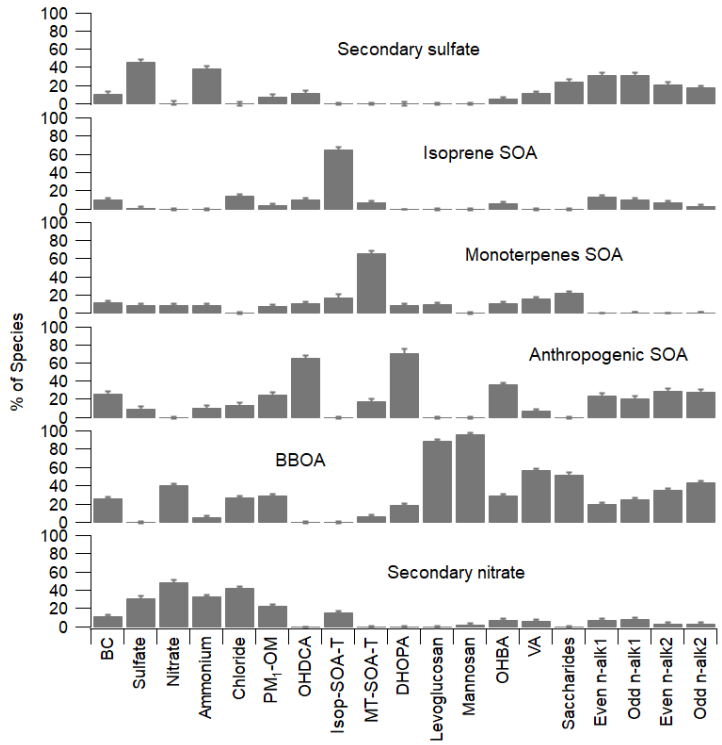

Figure 6. Source profiles of PM_1-OM. The errors are 95% CIs estimated by Bootstrap method.

Since PM_1-OM data were only available before 7 December, the source apportionment results were extended to the period of 7–19 December, by reconstructing PM_1-OM with individual source contributions. This approach is illustrated in Text S5, Figures S10-S11 and Tables S5-S6. In brief, it was based on the assumptions that the main tracers were still primarily attributed to the corresponding sources during 7–9 December, and their mass fractions in the total emissions of the corresponding sources did not significantly differ from those before 7 December. As a validation, the observed, PMF-predicted and reconstructed PM_1-OM are compared in Figure 7. Generally, both PMF and the reconstruction method reasonably reproduced the observed PM_1-OM. The linear regression of PMF-predicted PM_1-OM (reconstructed PM_1-OM) against observed PM_1-OM indicated a slope of 0.92 (0.90) and R^2 of 0.80 (0.62). As such, we adopted the reconstructed PM_1-OM and the corresponding contributions from individual sources. Due to the prevalence of continental air, the concentrations of primary air pollutants were significantly enhanced after 7 December, such as the ~4 and ~10 fold growth of NO_x and oleic acid, respectively. The unresolved POA components, including vehicle, ship and cooking emissions might make increased contributions to PM_1-OM in this period. Therefore, the PM_1-OM was most likely underestimated

after 7 December. It is hard to determine to what extent the unresolved OM (sum of PM_1-OM in factors of secondary sulfate and secondary nitrate) accounted for these POA components and their enhancements after 7 December. The uncertainties in source apportionment results related to the unresolved OM and potentially different sources during 7–19 December (*e.g.* cooking emissions) are discussed in Text S6. However, the conclusions on relative importance of the present sources would not change.

Bearing the uncertainties in mind, we conclude that BBOA contributed 8% – 74% (mean: 50±3%) to PM_1-OM in continental air, followed by anthropogenic SOA (12±1%), monoterpenes SOA (9±1%) and isoprene SOA (2±0.3%). The contributions of biogenic SOA might be underestimated, because some fractions of OHDCA potentially derived from biogenic VOCs in continental air were assigned to anthropogenic SOA. While the BBOA contributions were not quantifiable during 22 – 26 November due to the lack of levoglucosan data (days after passing of a cold front when continental air dominated), substantial increase in BBOA contributions occurred after 7 December. This was grounded upon the notable enhancements of levoglucosan in this period, as discussed in section 3.1. The significant contributions of BBOA in continental air induced by cold fronts were roughly comparable to those determined at a suburban site (~38%) [23] and at a mountainous site (~48%) [17] when Hong Kong was shrouded in regional air pollution. In contrast, the BBOA contributions (23±6%) were overwhelmed by those of anthropogenic SOA (37±4%) in marine air, so did those in mixed air (BBOA: 17±3% *vs.* anthropogenic SOA: 31±3%). It is interesting to note that both the time series and diurnal patterns of anthropogenic SOA were consistent with those of the more-oxidized oxygenated organic aerosols (MO-OOA) resolved by AMS, despite the overall lower concentrations of anthropogenic SOA resolved by TAG (Figure S13). This indicates the high oxidation state of anthropogenic SOA which might be inclined to stay in particles. The OMA with generally enhanced oxidative capacity might be sufficient in the passing air parcels to produce higher anthropogenic SOA in marine and mixed air. Like those in continental air, the biogenic SOA made minor contributions to PM_1-OM in marine air (11±1%) and mixed air (9±1%), which might be explained by the cool weather in this field campaign.

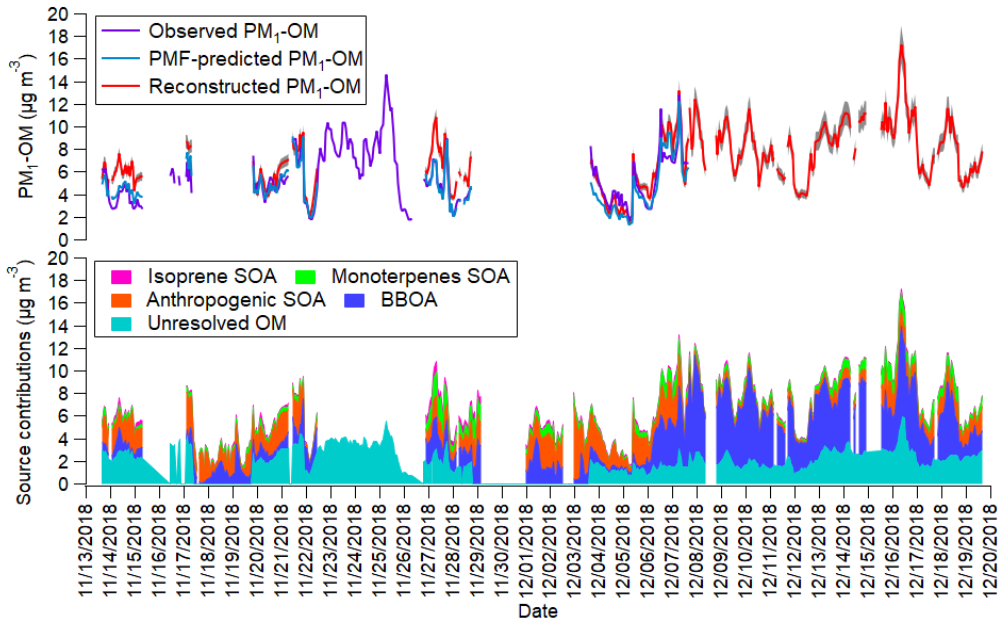

Figure 7. Time series of observed, PMF-predicted, reconstructed PM_1-OM, and contributions of individual sources to PM_1-OM. Grey area on red line of upper panel represents 95% CIs of the reconstructed PM_1-OM.

4. Implications

As a neighbor of mainland China and a coastal city facing SCS, Hong Kong air quality is very susceptible to regional transport of air pollution. Transient but severe air pollution episodes often occur in Hong Kong, causing rapid deterioration of air quality and acute exposures to toxic substances in the air. With the application of an in-situ analysis technique, this paper presents temporally resolved in-situ measurements of OA markers and the determination of changing contributions of specific sources to PM_1-OM. BB remains a significant contributor of OA in autumn in South China, though burning agricultural residuals had been strictly prohibited and levoglucosan concentrations indeed decreased compared to those in early 2000s. The temperature-dependent diurnal variations of levoglucosan in continental air suggest a shift of gas-to-particle partitioning might be an essential factor enhancing BBOA contributions in cool seasons. Even if marine or coastal air prevailed in Hong Kong, the residual BBOA above the PBL might still be transported down to the ground, increasing OA burdens. Since the two cold fronts caused strong continental outflows in this field campaign, we believe that the BBOA in continental air was

mainly attributable to regional rather than local sources. In addition, the "consensus" that marine air is relatively clean was challenged by our finding that the marine air was laden with anthropogenic SOA (mainly OHDCA), whose formation was likely facilitated by SO_2 and/or undetected pollutants in ship emissions. The abundant OHDCA in mixed air might also be attributable to the enhanced atmospheric oxidative capacity in OMA with the aging of continental outflows. Therefore, the OMA, where continental and marine air pollutants interacted, may be an ideal place for SOA formation. As a result, the air quality of coastal cities will be affected under sea breezes and have climatic consequences. The source apportionment failed to identify the expected vehicular, ship-emitted and cooking OA; however the findings of relative contributions of the present sources were still instructive. POA from regional BB and anthropogenic SOA possibly resulting from or at least enhanced by ship emissions should be controlled in cool seasons in Hong Kong.

Supporting Information

TAG operation procedures (Text S1); AMS calibrations and configurations (Text S2); Uncertainties associated with classification of air mass origins (Text S3); PMF configurations and modeling evaluation (Text S4); Reconstruction of PM_1-OM and method validation (Text S5); Uncertainties in source apportionment results (Text S6). Sampling site and instruments deployment (Figure S1); AMS collection efficiency calibration (Figure S2); Weather charts indicating cold fronts (Figure S3); Time series of BB tracers (Figure S4); Correlations between levoglucosan and acetonitrile/temperature (Figure S5); Diurnal patterns of O_x, oleic acid, PBL height and temperature (Figure S6); Q/Q_{exp} versus factor number (Figure S7); Source profiles in 5–7 factor solutions (Figure S8); Time series of scaled residuals (Figure S9); Relationships between source resolved PM_1-OM and tracers (Figure S10); Validation of reconstructed PM_1-OM (Figure S11); Diurnal patterns of unresolved OM, NO_x and SO_2 (Figure S12); Comparisons between anthropogenic SOA and MO-OOA (Figure S13). TAG development and application (Table S1); TAG operation parameters (Table S2); Quality control metrics of TAG data (Table S3); OA marker groups (Table S4); Instruments for auxiliary measurements (Table S5); Constraints applied to base run (Table S6); Bootstrap mapping results (Table S7).

Acknowledgements.

This study was supported by the Research Grants Council of the Hong Kong Special Administrative Region via Theme-Based Research Scheme (TRS) (Project T24-504/17-N), Collaborative Research Fund (CRF/C5004-15E), the Strategic Focus Area scheme of The

Research Institute for Sustainable Urban Development at The Hong Kong Polytechnic University (1-BBW9) and General Research Fund (PolyU 152052/14E and PolyU 152052/16E) of Research Grants Council of Hong Kong Special Administrative Region. The authors would like to thank the Hong Kong Environmental Protection Department for providing the trace gases and meteorological data. X.L. acknowledges technical advices on TAG operation from Qiongqiong Wang and Xiao He in Hong Kong University of Science and Technology, and Yutong Liang in University of California, Berkeley.

References:

[1] Kanakidou, M.; Seinfeld, J.H.; Pandis, S.N.; Barnes, I.; Dentener, F.J.; Facchini, M.C.; Dingenen, R.V.; Ervens, B.; Nenes, A.N.; Nielsen, C.J.; Swietlicki, E. Organic aerosol and global climate modelling: a review. *Atmos. Chem. Phys.* **2005**, 5(4), 1053-1123.

[2] Jimenez, J.L.; Canagaratna, M.R.; Donahue, N.M.; Prevot, A.S.; Zhang, Q.; Kroll, J.H.; DeCarlo, P.F.; Allan, J.D.; Coe, H.; Ng, N.L.; Aiken, A.C. Evolution of organic aerosols in the atmosphere. *Science*. **2009**, 326(5959), 1525-1529.

[3] Huang, R.J.; Zhang, Y.; Bozzetti, C.; Ho, K.F.; Cao, J.J.; Han, Y.; Daellenbach, K.R.; Slowik, J.G.; Platt, S.M.; Canonaco, F.; Zotter, P. High secondary aerosol contribution to particulate pollution during haze events in China. *Nature*. **2014**, 514(7521), 218-222.

[4] Goldstein, A.H.; Koven, C.D.; Heald, C.L.; Fung, I.Y. Biogenic carbon and anthropogenic pollutants combine to form a cooling haze over the southeastern United States. *Proc. Natl. Acad. Sci.* **2009**, 106(22), 8835-8840.

[5] Maria, S.F.; Russell, L.M.; Gilles, M.K.; Myneni, S.C. Organic aerosol growth mechanisms and their climate-forcing implications. *Science*. **2004**, 306(5703), 1921-1924.

[6] Mauderly, J.L.; Chow, J.C. Health effects of organic aerosols. *Inhal. Toxicol.* **2008**, 20(3), 257-288.

[7] Zhang, Q.; Zheng, Y.; Tong, D.; Shao, M.; Wang, S.; Zhang, Y.; Xu, X.; Wang, J.; He, H.; Liu, W.; Ding, Y. Drivers of improved $PM_{2.5}$ air quality in China from 2013 to 2017. *Proc. Natl. Acad. Sci.* **2019**, 116(49), 24463-24469.

[8] Chen, Q.; Fu, T.M.; Hu, J.; Ying, Q.; Zhang, L. Modelling secondary organic aerosols in China. *Natl. Sci. Rev.* **2017**, 4(6), 806-809.

[9] Cao, F.; Zhang, Y.; Ren, L.; Liu, J.; Li, J.; Zhang, G.; Liu, D.; Sun, Y.; Wang, Z.; Shi, Z.; Fu, P. New insights into the sources and formation of carbonaceous aerosols in China: potential applications of dual-carbon isotopes. *Natl. Sci. Rev.* **2017**, 4(6), 804-806.

[10] Jaeckels, J.M.; Bae, M.S.; Schauer, J.J. Positive matrix factorization (PMF) analysis of molecular marker measurements to quantify the sources of organic aerosols. *Environ. Sci. Technol.* **2007**, 41(16), 5763-5769.

[11] Fu, P.Q.; Kawamura, K.; Chen, J.; Charriere, B.; Sempere, R. Organic molecular composition of marine aerosols over the Arctic Ocean in summer: contributions of primary emission and secondary aerosol formation. *Biogeosciences*. **2013**, 10, 653-667.

[12] Ding, X.; Wang, X.; Xie, Z.; Zhang, Z.; Sun, L. Impacts of Siberian biomass burning on organic aerosols over the North Pacific Ocean and the Arctic: Primary and secondary organic tracers. *Environ. Sci. Technol.* **2013**, 47(7), 3149-3157.

[13] Wang, Q.; He, X.; Huang, X.H.; Griffith, S.M.; Feng, Y.; Zhang, T.; Zhang, Q.; Wu, D.; Yu, J.Z. Impact of secondary organic aerosol tracers on tracer-based source apportionment of organic carbon and $PM_{2.5}$: A case study in the Pearl River Delta, China. *ACS Earth Space Chem.* **2017**, 1(9), 562-571.

[14] Isaacman, G.; Kreisberg, N.M.; Yee, L.D.; Worton, D.R.; Chan, A.W.; Moss, J.A.; Hering, S.V.; Goldstein, A.H. Online derivatization for hourly measurements of gas-and particle-phase semi-volatile oxygenated organic compounds by thermal desorption aerosol gas chromatography (SV-TAG). *Atmos. Meas. Tech.* **2014**, 7(12), 4417-4429.

[15] Lee, B.P.; Li, Y.J.; Yu, J.Z.; Louie, P.K.; Chan, C.K. Physical and chemical characterization of ambient aerosol by HR-ToF-AMS at a suburban site in Hong Kong during springtime 2011. *J. Geophys. Res. Atmos.* **2013**, 118(15), 8625-8639.

[16] Sun, Y.L.; Zhang, Q.; Schwab, J.J.; Demerjian, K.L.; Chen, W.N.; Bae, M.S.; Hung, H.M.; Hogrefe, O.; Frank, B.; Rattigan, O.V.; Lin, Y.C. Characterization of the sources and processes of

526 organic and inorganic aerosols in New York city with a high-resolution time-of-flight aerosol mass
527 apectrometer. *Atmos. Chem. Phys.* **2011**, 11(4), 1581-1602.

528 [17] Lyu, X.P.; Guo, H.; Cheng, H.R.; Wang, X.M.; Ding, X.; Lu, H.X.; Yao, D.W.; Xu, C.
529 Observation of SOA tracers at a mountainous site in Hong Kong: Chemical characteristics, origins
530 and implication on particle growth. *Sci. Total Environ.* **2017**, 605, 180-189.

531 [18] Guo, H.; Ling, Z.H.; Cheung, K.; Jiang, F.; Wang, D.W.; Simpson, I.J.; Barletta, B.; Meinardi,
532 S.; Wang, T.J.; Wang, X.M.; Saunders, S.M. Characterization of photochemical pollution at
533 different elevations in mountainous areas in Hong Kong. *Atmos. Chem. Phys.* **2013**, 13(8), 3881-
534 3898.

535 [19] Zeren, Y.; Guo, H.; Lyu, X.; Jiang, F.; Wang, Y.; Liu, X.; Zeng, L.; Li, M.; Li, L. An ozone
536 "pool" in South China: Investigations on atmospheric dynamics and photochemical processes over
537 the Pearl River Estuary. *J. Geophys. Res. Atmos.* **2019**, 124(22), 12340-12355.

538 [20] Lyu, X.; Guo, H.; Simpson, I.J.; Meinardi, S.; Louie, P.K.; Ling, Z.; Wang, Y.; Liu, M.; Luk,
539 C.W.; Wang, N.; Blake, D.R. Effectiveness of replacing catalytic converters in LPG-fueled
540 vehicles in Hong Kong. *Atmos. Chem. Phys.* **2016**, 16(10), 6609-6626.

541 [21] Lee, B.P.; Li, Y.J.; Yu, J.Z.; Louie, P.K.; Chan, C.K. Characteristics of submicron particulate
542 matter at the urban roadside in downtown Hong Kong – Overview of 4 months of continuous
543 high‐resolution aerosol mass spectrometer measurements. *J. Geophys. Res. Atmos.* **2015**, 120(14),
544 7040-7058.

545 [22] Sun, C.; Lee, B.P.; Huang, D.; Li, Y.; Schurman, M.I.; Louie, P.K.; Luk, C.; Chan, C.K.
546 Continuous measurements at the urban roadside in an Asian megacity by Aerosol Chemical
547 Speciation Monitor (ACSM): particulate matter characteristics during fall and winter seasons in
548 Hong Kong. *Atmos. Chem. Phys.*, **2016**, 16(3), 1713-1728.

549 [23] Hu, D.; Bian, Q.; Lau, A.K.; Yu, J.Z. Source apportioning of primary and secondary organic
550 carbon in summer PM2.5 in Hong Kong using positive matrix factorization of secondary and
551 primary organic tracer data. *J. Geophys. Res. Atmos.* **2010**, 115(D16),
552 doi.org/10.1029/2009JD012498.

[24] Wong, Y.K.; Huang, X.H.; Yu, J.Z. Incorporating hopane degradation into chemical mass balance model: Improving accuracy of vehicular source contribution estimation. *Atmos. Environ.* **2019**, 210, 211-219.

[25] Williams, B.J.; Goldstein, A.H.; Kreisberg, N.M.; Hering, S.V. In situ measurements of gas/particle-phase transitions for atmospheric semivolatile organic compounds. *Proc. Natl. Acad. Sci.* **2010**, 107(15), 6676-6681.

[26] Zhao, Y.; Kreisberg, N.M.; Worton, D.R.; Isaacman, G.; Weber, R.J.; Liu, S.; Day, D.A.; Russell, L.M.; Markovic, M.Z.; VandenBoer, T.C.; Murphy, J.G. Insights into secondary organic aerosol formation mechanisms from measured gas/particle partitioning of specific organic tracer compounds. *Environ. Sci. Technol.* **2013**, 47(8), 3781-3787.

[27] Hunter, J.F.; Day, D.A.; Palm, B.B.; Yatavelli, R.L.; Chan, A.W.; Kaser, L.; Cappellin, L.; Hayes, P.L.; Cross, E.S.; Carrasquillo, A.J.; Campuzano-Jost, P. Comprehensive characterization of atmospheric organic carbon at a forested site. *Nat. Geosci.* **2017**, 10(10), 748-753.

[28] Zhao, Y.; Kreisberg, N.M.; Worton, D.R.; Isaacman, G.; Gentner, D.R.; Chan, A.W.; Weber, R.J.; Liu, S.; Day, D.A.; Russell, L.M.; Hering, S.V. Sources of organic aerosol investigated using organic compounds as tracers measured during CalNex in Bakersfield. *J. Geophys. Res. Atmos.* **2013**, 118(19), 11388-11398.

[29] Williams, B.J.; Goldstein, A.H.; Kreisberg, N.M.; Hering, S.V. An In-Situ Instrument for Speciated Organic Composition of Atmospheric Aerosols: Thermal Desorption Aerosol GC/MS-FID (TAG). *Aerosol Sci Technol.* **2006**, 40(8), 627-638.

[30] Goldstein, A.H.; Worton, D.R.; Williams, B.J.; Hering, S.V.; Kreisberg, N.M.; Panić, O.; Górecki, T. Thermal desorption comprehensive two-dimensional gas chromatography for in-situ measurements of organic aerosols. *J. Chromatogr. A.* **2008**, 1186(1-2), 340-347.

[31] Kreisberg, N.M.; Hering, S.V.; Williams, B.J.; Worton, D.R.; Goldstein, A.H. Quantification of hourly speciated organic compounds in atmospheric aerosols, measured by an in-situ Thermal desorption Aerosol Gas chromatograph (TAG). *Aerosol Sci Technol.* **2009**, 43(1), 38-52.

[32] Worton, D.R.; Kreisberg, N.M.; Isaacman, G.; Teng, A.P.; McNeish, C.; Górecki, T.; Hering, S.V.; Goldstein, A.H. Thermal desorption comprehensive two-dimensional gas chromatography:

An improved instrument for in-situ speciated measurements of organic aerosols. *Aerosol Sci Technol.* **2012**, 46(4), 380-393.

[33] Zhao, Y.; Kreisberg, N.M.; Worton, D.R.; Teng, A.P.; Hering, S.V.; Goldstein, A.H. Development of an in situ thermal desorption gas chromatography instrument for quantifying atmospheric semi-volatile organic compounds. *Aerosol Sci Technol.* **2013**, 47(3), 258-266.

[34] Isaacman, G.; Kreisberg, N.M.; Yee, L.D.; Worton, D.R.; Chan, A.W.; Moss, J.A.; Hering, S.V.; Goldstein, A.H. Online derivatization for hourly measurements of gas-and particle-phase semi-volatile oxygenated organic compounds by thermal desorption aerosol gas chromatography (SV-TAG). *Atmos. Meas. Tech.* **2014**, 7(12), 4417-4429.

[35] Williams, B.J.; Jayne, J.T.; Lambe, A.T.; Hohaus, T.; Kimmel, J.R.; Sueper, D.; Brooks, W.; Williams, L.R.; Trimborn, A.M.; Martinez, R.E.; Hayes, P.L. The first combined thermal desorption aerosol gas chromatograph–Aerosol mass spectrometer (TAG-AMS). *Aerosol Sci Technol.* **2014**, 48(4), 358-370.

[36] Ren, H.; Xue, M.; An, Z.; Zhou, W.; Jiang, J. Quartz filter-based thermal desorption gas chromatography mass spectrometry for in-situ molecular level measurement of ambient organic aerosols. *J. Chromatogr. A.* **2019**, 1589, 141-148.

[37] Ren, H.; Xue, M.; An, Z.; Jiang, J. Improving thermal desorption aerosol gas chromatography using a dual-trap design. *J. Chromatogr. A.* **2019**, 1599, 247-252.

[38] An, Z.; Ren, H.; Xue, M.; Guan, X.; Jiang, J. Comprehensive Two-Dimensional Gas Chromatography Mass Spectrometry with a Solid-state Thermal Modulator for In-situ Speciated Measurement of Organic Aerosols. *J. Chromatogr. A.* **2020**, doi.org/10.1016/j.chroma.2020.461336.

[39] Zhang, Y.N.; Zhang, Z.S.; Chan, C.Y.; Engling, G.; Sang, X.F.; Shi, S.; Wang, X.M. Levoglucosan and carbonaceous species in the background aerosol of coastal southeast China: case study on transport of biomass burning smoke from the Philippines. *Environ. Sci. Pollut. Res.* **2012**, 19(1), 244-255.

[40] Wang, T.; Dai, J.; Lam, K.S.; Poon, C.; Brasseur, G.P. Twenty-Five Years of Lower Tropospheric Ozone Observations in Tropical East Asia: The Influence of Emissions and Weather Patterns. *Geophys. Res. Lett.* **2019**, 46(20), 11463-11470.

[41] Hu, D.; Bian, Q.; Li, T.W.; Lau, A.K.; Yu, J.Z. Contributions of isoprene, monoterpenes, β-caryophyllene, and toluene to secondary organic aerosols in Hong Kong during the summer of 2006. *J. Geophys. Res. Atmos*. **2008**, 113(D22), doi.org/10.1029/2008JD010437.

[42] Hu, D.; Yu, J.Z. Secondary organic aerosol tracers and malic acid in Hong Kong: seasonal trends and origins. *Environ. Chem.* **2013**, 10(5), 381-394.

[43] Simoneit, B.R.; Schauer, J.J.; Nolte, C.G.; Oros, D.R.; Elias, V.O.; Fraser, M.P.; Rogge, W.F.; Cass, G.R. Levoglucosan, a tracer for cellulose in biomass burning and atmospheric particles. *Atmos. Environ.* **1999**, 33(2), 173-182.

[44] Zheng, M.; Hagler, G.S.; Ke, L.; Bergin, M.H.; Wang, F.; Louie, P.K.; Salmon, L.; Sin, D.W.; Yu, J.Z.; Schauer, J.J. Composition and sources of carbonaceous aerosols at three contrasting sites in Hong Kong. *J. Geophys. Res. Atmos.* **2006**, 111(D20), doi.org/10.1029/2006JD007074.

[45] Ding, X.; Wang, X.M.; Gao, B.; Fu, X.X.; He, Q.F.; Zhao, X.Y.; Yu, J.Z.; Zheng, M. Tracer–based estimation of secondary organic carbon in the Pearl River Delta, south China. *J. Geophys. Res. Atmos.* **2012**, doi.org/10.1029/2011JD016596.

[46] Schauer, J.J.; Kleeman, M.J.; Cass, G.R.; Simoneit, B.R. Measurement of emissions from air pollution sources. 4. C1− C27 organic compounds from cooking with seed oils. *Environ. Sci. Technol.* **2002**, 36(4), 567-575.

[47] Holzinger, R.; Warneke, C.; Hansel, A.; Jordan, A.; Lindinger, W.; Scharffe, D.H.; Schade, G.; Crutzen, P.J. Biomass burning as a source of formaldehyde, acetaldehyde, methanol, acetone, acetonitrile, and hydrogen cyanide. *Geophys. Res. Lett.* **1999**, 26(8), 1161-1164.

[48] Schneider, J.; Weimer, S.; Drewnick, F.; Borrmann, S.; Helas, G.; Gwaze, P.; Schmid, O.; Andreae, M.O.; Kirchner, U. Mass spectrometric analysis and aerodynamic properties of various types of combustion-related aerosol particles. *Int. J. Mass Spectrom.* **2006**, 258(1-3), 37-49.

[49] Logan, J.A.; Prather, M.J.; Wofsy, S.C.; McElroy, M.B. Tropospheric chemistry: A global perspective. *J. Geophys. Res. Oceans.* **1981**, 86(C8), 7210-7254.

[50] Kleinman, L.I. Low and high NOx tropospheric photochemistry. *J. Geophys. Res. Atmos*. **1994**, 99(D8), 16831-16838.

[51] Wang, H.; Lyu, X.P.; Guo, H.; Wang, Y.; Zou, S.C.; Ling, Z.H.; Wang, X.M.; Jiang, F.; Zeren, Y.Z.; Pan, W.Z.; Huang, X.B. Ozone pollution around a coastal region of South China Sea: interaction between marine and continental air. *Atmos. Chem. Phys.* **2018**, 18, 4277-4295.

[52] Wang, Y.; Guo, H.; Zou, S.; Lyu, X.; Ling, Z.; Cheng, H.; Zeren, Y. Surface O_3 photochemistry over the South China Sea: Application of a near-explicit chemical mechanism box model. *Environ. Pollut*. **2018**, 234, 155-166.

[53] Lobit, P.; Genard, M.; Soing, P.; Habib, R. Modelling malic acid accumulation in fruits: relationships with organic acids, potassium, and temperature. *J. Exp. Bot.* **2006**, 57(6), 1471-1483.

[54] Kawamura, K.; Sakaguchi, F. Molecular distributions of water soluble dicarboxylic acids in marine aerosols over the Pacific Ocean including tropics. *J. Geophys. Res. Atmos.* **1999**, 104(D3), 3501-3509.

[55] Ervens, B.; Feingold, G.; Frost, G.J.; Kreidenweis, S.M. A modeling study of aqueous production of dicarboxylic acids: 1. Chemical pathways and speciated organic mass production. *J. Geophys. Res. Atmos.* **2004**, 109(D15), doi.org/10.1029/2003JD004387.

[56] Claeys, M.; Wang, W.; Ion, A.C.; Kourtchev, I.; Gelencsér, A.; Maenhaut, W. Formation of secondary organic aerosols from isoprene and its gas-phase oxidation products through reaction with hydrogen peroxide. *Atmos. Environ.* **2004**, 8(25), 4093-4098.

[57] Riva, M.; Budisulistiorini, S.H.; Zhang, Z.; Gold, A.; Surratt, J.D. Chemical characterization of secondary organic aerosol constituents from isoprene ozonolysis in the presence of acidic aerosol. *Atmos. Environ.* **2016**, 130, 5-13.

[58] *Hong Kong Air Pollutant Emission Inventory – Sulphur Dioxide* Website; https://www.epd.gov.hk/epd/english/environmentinhk/air/data/emission_inve_so2_C.html, lastly accessed on 27 June 2020.

[59] Xu, L.; Guo, H.; Boyd, C.M.; Klein, M.; Bougiatioti, A.; Cerully, K.M.; Hite, J.R.; Isaacman-VanWertz, G.; Kreisberg, N.M.; Knote, C.; Olson, K. Effects of anthropogenic emissions on aerosol formation from isoprene and monoterpenes in the southeastern United States. *Proc. Natl. Acad. Sci.* **2015**, 112(1), 37-42.

[60] Williams, B.J.; Goldstein, A.H.; Millet, D.B.; Holzinger, R.; Kreisberg, N.M.; Hering, S.V.; White, A.B.; Worsnop, D.R.; Allan, J.D.; Jimenez, J.L. Chemical speciation of organic aerosol during the International Consortium for Atmospheric Research on Transport and Transformation 2004: Results from in situ measurements. *J. Geophys. Res. Atmos.* **2007**, doi.org/10.1029/2006JD007601.

[61] Williams, B.J.; Goldstein, A.H.; Kreisberg, N.M.; Hering, S.V.; Worsnop, D.R.; Ulbrich, I.M.; Docherty, K.S.; Jimenez, J.L. Major components of atmospheric organic aerosol in southern California as determined by hourly measurements of source marker compounds. *Atmos. Chem. Phys.* **2010**, 10(23), 11577-11603.

[62] Worton, D.R.; Goldstein, A.H.; Farmer, D.K.; Docherty, K.S.; Jimenez, J.L.; Gilman, J.B.; Kuster, W.C.; De Gouw, J.; Williams, B.J.; Kreisberg, N.M.; Hering, S.V. Origins and composition of fine atmospheric carbonaceous aerosol in the Sierra Nevada Mountains, California. *Atmos. Chem. Phys.* **2011**, 11(19), 10219-10241.

[63] Chan, A.W.; Kreisberg, N.M.; Hohaus, T.; Campuzano-Jost, P.; Zhao, Y.; Day, D.A.; Kaser, L.; Karl, T.; Hansel, A.; Teng, A.P.; Ruehl, C.R. Speciated measurements of semivolatile and intermediate volatility organic compounds (S/IVOCs) in a pine forest during BEACHON-RoMBAS 2011. *Atmos. Chem. Phys.* **2016**, 16(2), 1187-1205.

[64] Lambe, A.T.; Logue, J.M.; Kreisberg, N.M.; Hering, S.V.; Worton, D.R.; Goldstein, A.H.; Donahue, N.M.; Robinson, A.L. Apportioning black carbon to sources using highly time-resolved ambient measurements of organic molecular markers in Pittsburgh. *Atmos. Environ.* **2009**, 43(25), 3941-3950.

[65] Zielinska, B.; Sagebiel, J.; McDonald, J.D.; Whitney, K.; Lawson, D.R. Emission rates and comparative chemical composition from selected in-use diesel and gasoline-fueled vehicles. *J. Air Waste Manage. Assoc.* **2004**, 54(9), 1138-1150.

689 [66] Ding, X.; Zhang, Y.Q.; He, Q.F.; Yu, Q.Q.; Wang, J.Q.; Shen, R.Q.; Song, W.; Wang, Y.S.;
690 Wang, X.M. Significant increase of aromatics-derived secondary organic aerosol during fall to
691 winter in China. Environmental science & technology. 51(13):7432-7441, 2017.

692 [67] Fabbri, D.; Torri, C.; Simoneit, B.R.; Marynowski, L.; Rushdi, A.I.; Fabiańska, M.J.
693 Levoglucosan and other cellulose and lignin markers in emissions from burning of Miocene
694 lignites. *Atmos. Environ.* **2009**, 43(14), 2286-2295.